Computational Materials Science 228 (2023) 112346

Contents lists available at ScienceDirect

Computational Materials Science

journal homepage: www.elsevier.com/locate/commatsci

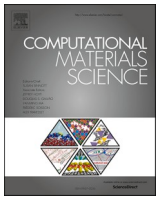

Full Length Article

Molecular Dynamics study on buckling behavior of vertically aligned carbon nanotube (VACNT) bundles with characterized waviness

Aghyad B. Al Tahhan [a], Mohammad Alkhedher [a,*], Abdel-Hamid I. Mourad [b], Mohamad Ramadan [c,d], Mutasem A. Shehadeh [e]

[a] Department of Mechanical and Industrial Engineering, Abu Dhabi University, Abu Dhabi, PO 59911, United Arab Emirates
[b] Mechanical Engineering Department, United Arab Emirates University, Al-Ain, P.O. Box 17555, United Arab Emirates
[c] School of Engineering, International University of Beirut BIU, Beirut, Lebanon
[d] School of Engineering, Lebanese International University LIU, Bekaa, Lebanon
[e] Department of Mechanical Engineering, Al Faisal University, Riyadh, Saudi Arabia

ARTICLE INFO

Keywords:
Carbon nanotubes
Molecular Dynamics
Buckling
VACNT
Curvature
Nanotube bundle

ABSTRACT

The buckling behavior of vertically aligned carbon nanotube (VACNT) bundles with a characterized waviness ratio was studied using the principle of sinusoidal waves. A MATLAB algorithm was used to generate bundles with a user-specified waviness ratio, and 12 VACNT models were used under a constant strain of 0.01/ps uniaxial compression with three variable parameters: waviness ratio, number of VACNTs within the bundle, and presence of van der Waals interactions; moreover, the findings suggest that these parameters significantly influenced the critical buckling stress (σ_{comp}) and buckling behavior of the bundle. Increasing the waviness resulted in a significant reduction of approximately 59.96% between a bundle with no waviness and a bundle with a waviness ratio of 0.33. Including van der Waals interactions played a critical role in strengthening the overall VACNT bundle, whereas eliminating them changed the buckling pattern and behavior of the bundles, furthermore, increasing the number of VACNTs in a bundle increased the critical buckling stress of the overall bundle. This study provides insight into the structural behavior of VACNT bundles, which is expected to impact the design of any system in which the collective mechanical behavior of the VACNT bundles is critical. These findings can improve the study of composite materials in lithium-ion batteries for high-capacity CNT composite anodes.

1. Introduction

Since the discovery of carbon nanotubes (CNT) by Iijima [1], researchers have been motivated to study and analyze their remarkable properties. This finding opened the doors for further experimentation and design of nanostructures using carbon nanotubes and amplified the interest in CNTs. Most theoretical analyses have focused on the mechanical [2], thermal [3], and electrical properties [4] of pristine single-walled carbon nanotubes (SWCNT) and multi-walled carbon nanotubes (MWCNT). However, carbon nanotubes are synthesized in different forms; one of the forms is the Vertically Aligned CNT (VACNT) bundles, where individual CNTs are closely packed together to form a large CNT bundle [5]. Bedewy et al. [6] observed that carbon nanotubes synthesized on a high-density substrate usually self-organize into vertically aligned formations. Characterizing the properties of the VACNT bundle is very important, as it allows researchers to interpret the various applications and designs of CNTs. Studying CNTs in the form of VACNTs has attracted the interest of many researchers owing to their super compressible response and strong resilience [7]. The overall buckling strength of the VACNTs bundles allows the bundles to deform and recover simultaneously under various compression loading scenarios. The inter-tube interactions between CNTs in a bundle can be non-bonded Van der Waals (VdW) interactions and bonded interactions [5,8].

Studies have focused on individual CNTs; however, recently, the analysis of CNT arrays has become of interest compared with experimental and numerical studies on individual CNTs. Liew et al. [9,10] studied tensile and compressive mechanical properties of CNT bundles using Molecular Dynamics (MD) simulations. In their study, they observed that nanotube bundle tensile or compressive failure load could be determined from the collective failure loads of the individual CNT within the bundle. Furthermore, the presence of Van der Waals

* Corresponding author.
E-mail address: Mohammad.alkhedher@adu.ac.ae (M. Alkhedher).

https://doi.org/10.1016/j.commatsci.2023.112346
Received 11 March 2023; Received in revised form 23 May 2023; Accepted 16 June 2023
Available online 1 July 2023

interactions tends to weaken the mechanical loading performance of the CNT bundles. Li et al. [11] observed experimentally that the buckling behavior of VACNT bundles differs from the suggested Euler column buckling model for individual CNTs under axial compression, which was also employed by Cao et al. [7] and Zbib et al. [12]. This difference was attributed to the presence of VdW interactions, which can significantly influence the buckling behavior of VACNT bundles, which may affect the load-carrying capacity and failure loads of the bundle. Most experimental studies on VACNT bundles under compressive loading showed that they begin to buckle near the substrate region [12,13]. By contrast, Maschmann et al. [14] reported the propagation of folds near the top surface of an indented bundle. In their study, VACNTs exhibited open-cell foam behavior under a flat punch indentation with fluctuations in compressive force measurements. A thorough understanding of the buckling behavior of VACNT bundles allows for expanding the possibility of using CNT bundles in nano-electromechanical applications, such as torsional springs, actuators, and nano-oscillators [15,16,17]. CNTs are highly susceptible to buckling and deformation in such applications owing to their long, wavy, and hollow tubular structures. Thus, it is critical to fully understand the mechanical performance of the VACNT bundles under compressive loading.

CNTs have been thoroughly studied under tensile loading [18,19], bending [20], and twisting [10]. However, the experimental uniaxial compression of CNT bundles has been challenging because of the difficulty in attaining perfectly aligned uniaxial loading on the bundle's structure. Researchers have utilized different approaches to model compressive loading on carbon nanotubes; for example, Waters et al. [21] studied the buckling instabilities of VACNTs using a nano-indenter to induce uniaxial compression. Similarly, Liang et al. [22] observed the compression and recovery of CNT forests using a MEMS-based silicon capacitive load cell for uniaxial compression testing and a slightly different setup for nanoindentation. In their conclusion, the buckling behavior of CNT forests was defined as reversible, where they can act like springs. However, Molecular Dynamics (MD) simulations can provide a better understanding of the mechanical properties of VACNT bundles, which is because, in MD, the material structure is modeled as a number of atoms with their respective molecular interactions [5,23]. Furthermore, when modeling carbon nanotubes in MD simulations, the interactions of each atom can be quantified by a gradient of the total potential energy based on the interatomic function used. MD simulations allow researchers to examine the influence of different parameters that can affect the collective strength of the VACNT bundles. These parameters can include multiple structural modifications, such as missing nanotubes, waviness along the nanotube axis, and the total number of tubes in a bundle.

CNTs are usually grown with random waviness along their axes, as observed in various SEM images [24,25]. Several simulation studies have shown that curvature variation along the axis of CNTs hinders their mechanical properties. In an MD study by Al Tahhan et al. [26], the increased waviness of a CNT structure was shown to decrease its ultimate tensile strength compared with straight CNTs. Similarly, Wong et al. [27] studied the buckling characteristics of several curved forms of CNTs and compared the results to those of pristine and straight CNTs under axial compression. In their study, C-shaped- and S-shaped CNTs were assessed under similar testing conditions. The buckling load of the C-shaped CNTs was 43 nN, whereas its straight counterpart had a buckling load of approximately 72 nN. Therefore, the load-carrying capacity of the C-shaped CNT decreased by approximately 40%. An example of a wavy carbon nanotube VACNT compared to a straight VACNT is shown in Fig. 1. The effects of such curvature on CNT bundles have also been systematically studied in the context of compressive strength.

This study emphasizes the influence of waviness on the compressive load capacity of VACNT bundles and their buckling behavior under axial compression. Additionally, the influence of activating the vdW interactions between the tubes within a bundle on the buckling performance of the overall bundle was examined. Wong et al. [27] examined a similar study on individual SWCNT samples using MD simulation and highlighted the effect of curvature on their final performance. However, it was also reported that the wavy CNTs, combined with other CNTs to form a nanotube bundle, weaken the bundle's collective mechanical performance. The effects of such waviness on the CNT bundles have also been systematically studied in the context of compressive strength and presented.

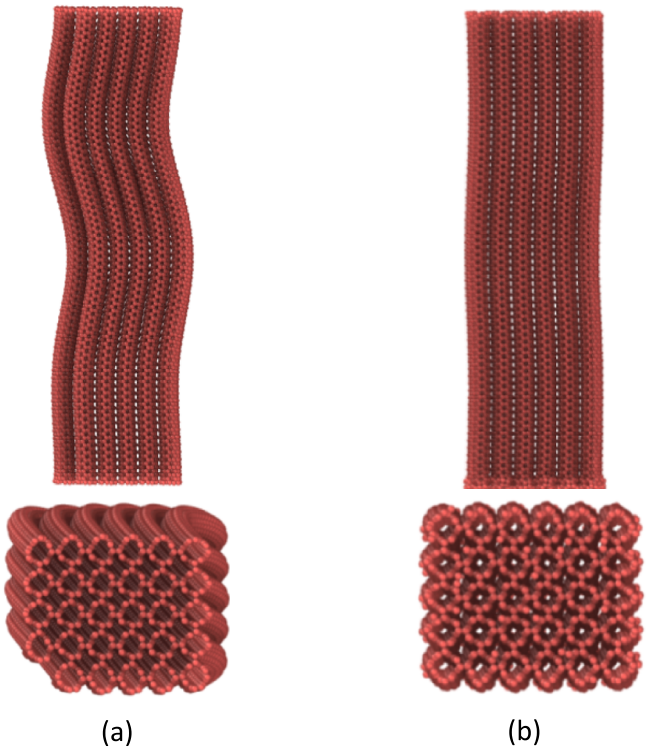

Fig. 1. A) sample atomic structure of a wavy vacnt bundle. b) sample atomic structure of a straight vacnt bundle.

2. Atomistic modeling of wavy VACNT bundles

Ginga et al. [28] observed that the waviness present in VACNT forests significantly reduces their stiffness. In previous MD studies, carbon nanotube structures were modeled as pristine straight tubes of different lengths and walls [5,23,29]. The development of an accurate and stable atomic structure is critical for MD simulations because instability in the MD data file can hinder the accuracy of the simulation results. The development of an accurate and stable atomic structure is a critical part of MD simulations because instability in the MD data file can hinder the accuracy of the simulation results. In previous MD studies, carbon nanotube structures have been modeled as pristine straight tubes of different lengths and walls [5,23,29]. However, Ginga et al. [28] observed that the waviness present in VACNT forests significantly reduced their stiffness. Furthermore, based on various scanning electron microscope (SEM) images retrieved from Al-Khedher et al. [30] shown below:

As observed in Fig. 2, waviness is always present in VACNTs, regardless of the fabrication method and its control. Therefore, it is an important variable to implement in VACNT studies. Previous studies have reported that the compliance of VACNT forests subjected to mechanical loading is a result of their buckling or bending. However, in the analytical model proposed by [28], it was concluded that the high compliance of the VACNT forest under various loading modes was due to the waviness of individual CNTs within. Hence, in this study, the forest

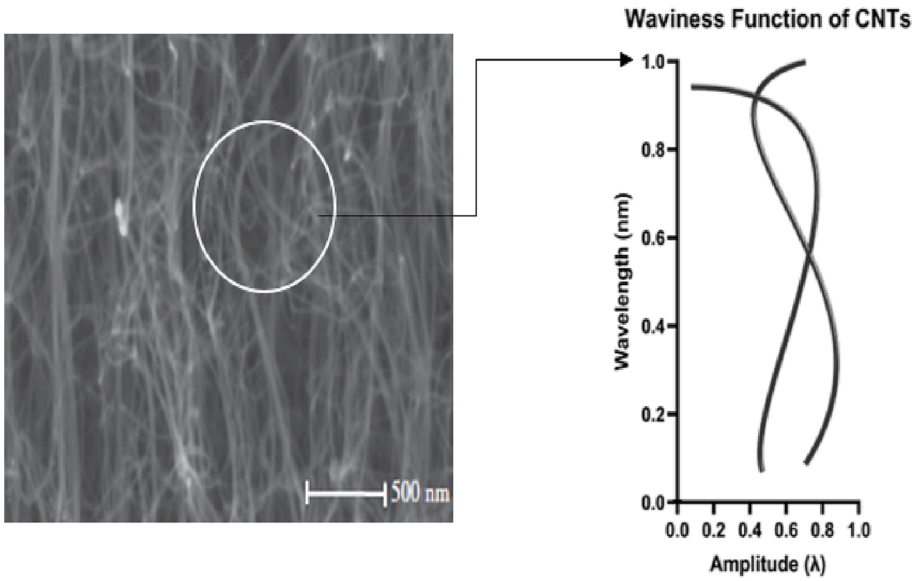

Fig. 2. SEM image of a CNT forest [30] with an expansion of the mathematical characterization of waviness along the axis of the CNTs to the right of the image. (l) is the wavelength of the tube along the y-axis in 2D space, and (λ) represents the wave amplitude along the x-axis. Waviness is the ratio of both variables.

was modeled using an extension of the MATLAB Algorithm used in [26]. The algorithm uses a spline of defined curvature and smoothens it to eliminate sharp bends. After the spline is modeled, the code imports the coordinates of a straight carbon nanotube generated using VMD and fits the atoms layer-by-layer to the spline curve. The initial output of the model is an individual carbon nanotube with a specified curvature output in the (.XYZ) format data file. After the wavy CNT coordinates were recorded, the model utilized an incremental alignment method to place the CNTs in a square-shaped forest. Array dimensions were defined by the number of tubes aligned or inserted. For example, a 6 × 6 square VACNT array is dimensioned at 3.6 nm by 3.6 nm with 36 wavy CNTs. A sample of the operational pattern of the algorithm is shown in Fig. 3.

Many approaches have analytically modeled the waviness of CNTs, and different curved CNT morphologies have been discussed in the literature to characterize the wavy state of CNTs. Fisher et al. [31] modeled the waviness in CNTs as planar sinusoidal waves. Zeng et al. [32], represented the waviness of the CNT as connected polyline segments with straight ends. Stein et al. [33] investigated the influence of waviness on the elastic properties of VACNTs in a polymer matrix. Their approach to waviness was determined by examining the random wavy morphology of the CNT array using SEM imaging. Furthermore, they modeled waviness using a simple sinusoidal wave model and quantified waviness using the waviness ratio w. The waviness in the CNT structure was shown to be very influential on the overall mechanical performance of VACNT arrays, and studies have shown that the CNT waviness, quantified via the waviness ratio (w), is responsible for a major reduction in the effective CNT stiffness [34].

$$y = w\cos\left(\frac{2\pi z}{l}\right) at\, z \in [0, \lambda \tag{1}$$

In this work, the waviness of the carbon nanotubes is modeled using the following sinusoidal mathematical formulation that is built on the waviness ratio assumption highlighted in Fig. 2 as per [35]:

where (a) and (l) are the amplitude and the wavelength of the wavy nanotube, respectively. The parameter $w = \frac{a}{l}$ is the waviness ratio, which defines the degree of curvature of the nanotube. The waviness ratio (w) is set within the algorithm by specifying the wavelength and amplitude of the CNT structure. Four models were generated, three of which represented a varying range of CNTs curvatures, as shown in Fig. 4. Additionally, only half of a complete sine-curved nanotube was considered in the MD simulations. Three curved single-walled CNTs were generated and equilibrated before use in the simulation.

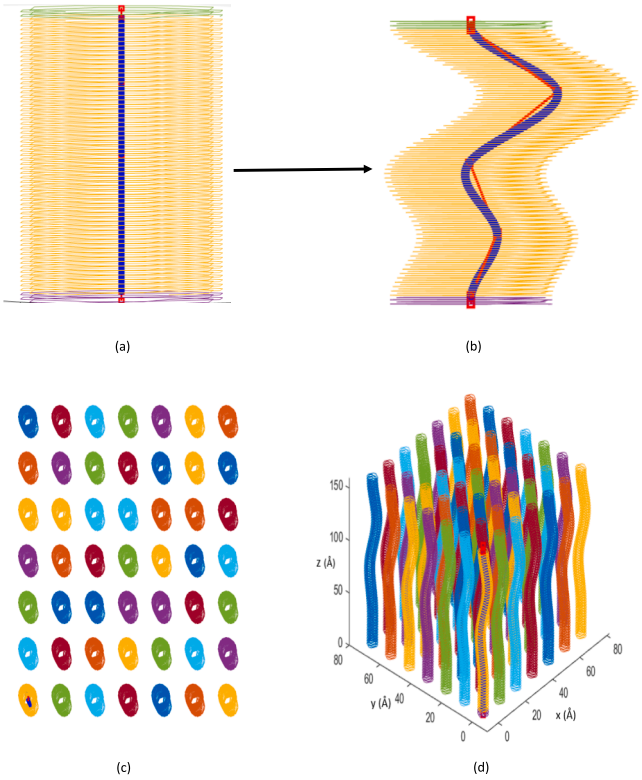

Fig. 3. Process of generating a VACNT bundle using MATLAB a) importing a straight CNT structure. b) The straight structure was fitted into a wavy spline that mimicked the waviness of the CNTs. c) The wavy CNT was then placed in a rectangular grid specified by the user and aligned with a specific grid spacing. d) Isometric view of the final VACNT bundle.

All nanotubes were selected to be (5,5) armchair SWCNT of length (L) 15.9 nm and a diameter of (D) = 6.785 Å or 0.6785 nm and an intertube spacing (a) of 0.68 nm. Finally, Table 1 highlights the forest types used in the simulation, with their accompanying illustrations.

A sample illustration of the bundle size differences is shown in Fig. 5.

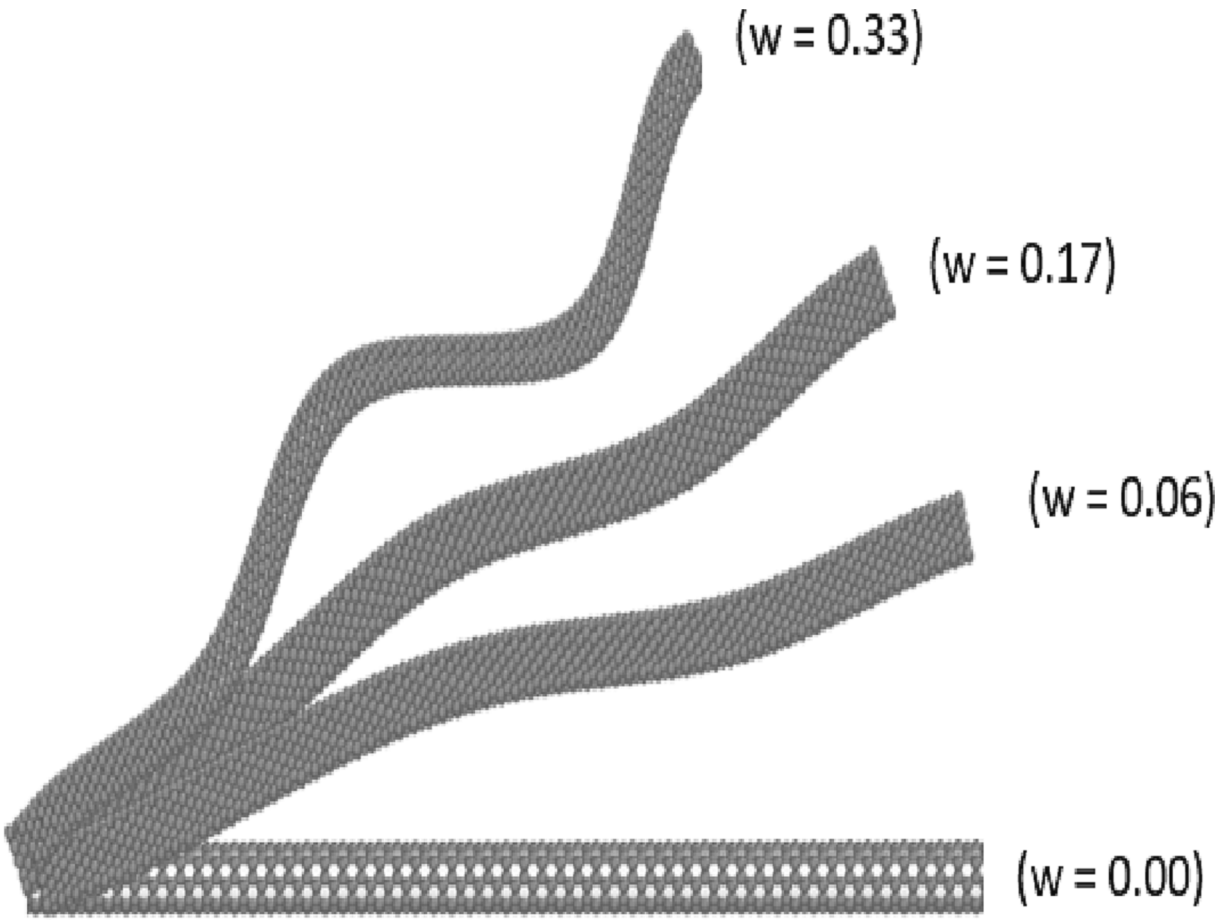

Fig. 4. The study included various CNT structures with different ranges of waviness quantified by the waviness ratio (w), which is defined as $w = \frac{a}{l}$.

Table 1
Specifications of the samples used in the study.

Sample Group No.	Waviness Ratio (w)	L/D	N_{CNT}
1	0.06	23.43	30
	0.17		
	0.33		
2	0.17	23.43	50
3	0.17	23.43	80

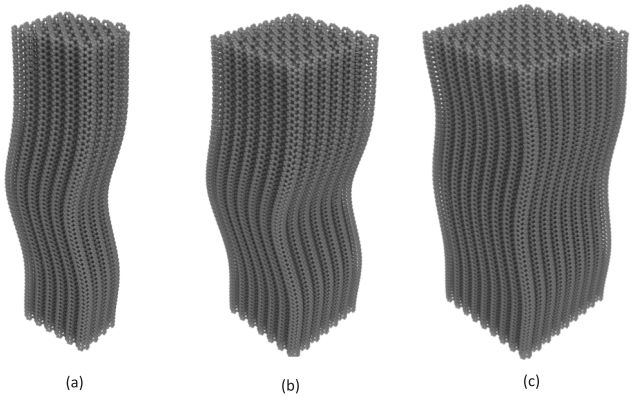

Fig. 5. W-VACNT samples used in the MD study (w = 0.17) (a) $N_{CNT} = 30$ (b) $N_{CNT} = 50$c) $N_{CNT} = 80$.

The importance of varying the number of nanotubes (N_{CNT}) in the bundle is to observe the load-carrying capacity of the bundle as a function of the CNTs number or bundle size [5].

3. Molecular Dynamics study parameters and methods

This study was performed using classical molecular dynamics using the LAMMPS simulation environment. The general concept behind this study was to simulate compressive loading on the generated W-VACNT bundles to visualize the buckling behavior in the bundle and the influence of waviness on its ultimate compressive load-carrying capacity. The intra-and intermolecular interactions between atoms are an integral part of atomistic simulations. Therefore, at the initial stages, the Adaptive Intermolecular Reactive Empirical Bond Order (AIREBO) potential was used to model the intermolecular interactions between the carbon nanotube C–C bonds. The mathematical formulation of the AIREBO potential is highlighted below [36]:

$$\mathbf{E} = \frac{1}{2}\sum_{\mathbf{i}}\sum_{\mathbf{j}\neq\mathbf{i}}\left[\mathbf{E}_{\mathbf{ij}}^{\mathbf{REBO}} + \mathbf{E}_{\mathbf{ij}}^{\mathbf{LJ}} + \sum_{\mathbf{K}\neq\mathbf{i},\mathbf{jl}\neq\mathbf{i},\mathbf{j},\mathbf{k}}\sum \mathbf{E}_{\mathbf{kijl}}^{\mathbf{TORSION}}\right] \quad (2)$$

where E is the total potential energy of the system, $\mathbf{E}_{\mathbf{ij}}^{\mathbf{REBO}}$ is the REBO energy, $\mathbf{E}_{\mathbf{ij}}^{\mathbf{LJ}}$ Lennard-Jones Energy, and $\mathbf{E}_{\mathbf{kijl}}^{\mathbf{TORSION}}$ is the torsion energy. The AIREBO potential allows the implementation of VdW interactions that hold the carbon nanotube together in a bundle. Earlier studies on CNT bundles have utilized Brenner's short-range second-generation REBO potential [10]. However, the REBO potential doesn't include the vdW interactions and requires coupling the $\mathbf{E}_{\mathbf{ij}}^{\mathbf{REBO}}$ with the long-range non-bonded vdW force F_{vdW}.

Furthermore, in the coupling process, the long-range Van der Waals interaction is approximated by the Lennard-Jones (12,6) potential highlighted in the formulation below in Equation 3 [37,38]:

$$\mathbf{E}^{\mathbf{LJ}} = 4\boldsymbol{\xi}\left[\left(\frac{\boldsymbol{\sigma_{ij}}}{\boldsymbol{r}}\right)^{12} - \left(\frac{\boldsymbol{\sigma_{ij}}}{\boldsymbol{r}}\right)^{6}\right] \tag{3}$$

where $\boldsymbol{\xi}$ is the well depth of the potential and $\boldsymbol{\sigma_{ij}}$ is the collision diameter between two atoms. Therefore, the combined total energy expression that resulted from coupling the short-range interactions represented by the REBO potential and the long-range interactions characterized by equation 3 can be highlighted below in equation 4:

$$\mathbf{E} = \sum_{\mathbf{i}}\sum_{\mathbf{j}>\mathbf{i}}\left[\mathbf{E}_{\mathbf{ij}}^{\mathbf{REBO}} + \mathrm{E}_{\mathrm{vdw}}\right] \tag{4}$$

Using the AIREBO potential users have the capability of turning the Lennard–Jones interactions on/off, which provides the opportunity to examine the influence of the vdW interaction in large W-VACNT bundles without having to undergo the coupling process proposed earlier [36,39]. Later, MD simulations were performed on W-VACNT bundles undergoing axial compressive loading. Axial compressive loads were achieved by introducing a negative strain rate of 0.01/ps [5] to the top of the CNT bundles, as shown in Fig. 6. During loading, all the atoms are at one end. Axial compression (i.e., compression) is applied to all atoms within the bundle on the moving end, while the other displacements (i.e., X- and Y-direction displacements) are kept free.

Furthermore, as previously illustrated in the representation of the W-VACNT bundle in Fig. 3, The SWCNTs in the CNT bundle are spaced 0.68 nm apart, and the length of the bundle ish_b = 15.9 nm. The diameter of each (5,5) SWCNT wasD_t = 0.6785 nm and each CNT bundle consisted of 31440, 52400, and 84,840 atoms, respectively. The simulation system was divided into three stages: energy minimization, relaxation, and compressive loading. During the minimization stage, the atom coordinates are iteratively adjusted to achieve a local potential energy minimum with a maximum force-stopping tolerance of 10^{-12} eV/Å. It is important to note that the minimization process does not necessarily yield an exact local minimum. The value is approximated at a critical point, as per the following objective function highlighted by Equation 5, which is the total potential energy of the system as a function of the N atoms coordinates [40].

$$\begin{aligned}\mathbf{E}(\mathbf{r}_1, \mathbf{r}_2, \cdots, \mathbf{r}_\mathbf{N}) = &\sum_{\mathbf{i,j}} E_{pair}(r_i, r_j) + \sum_{ij} E_{bond}(r_i, r_j) + \sum_{ijk} E_{angle}(r_i, r_j, r_k) \\ &+ \sum_{ijkl} E_{dihedral}(r_i, r_j, r_k, r_l) + \sum_{ijkl} E_{improper}(r_i, r_j, r_k, r_l) + \sum_{i} E_{fix}(r_i)\end{aligned} \tag{5}$$

where E_{pair} is the sum of all non-bonded pairwise interactions and E_{bond}, E_{angle}, $E_{dihedral}$, and ($E_{improper}$) are the bond, angle, dihedral, and improper interactions respectively. Finally, the last term (E_{fix}) is energy owing to fixes that can act as constraints or apply force to atoms, for example, through interaction with a surface. In the relaxation stage, To aid in equilibration, the W-VACNT bundle was subjected to a random displacement in the X, Y, and Z direction. This is done using the velocity command to allow the W-VACNT bundle to reach a target temp(T_{target})of 300 K. The temperature is then maintained using the Nose/Hoover thermostat. Later, the bundle is relaxed for 10,000 steps at a timestep value of dt = 0.001 ps with an NPT ensemble imposed on the structure. The third stage involves imposing another NPT ensemble and then applying incremental deformation at the engineering strain rate [41]. Furthermore, the temperature was kept constant within the simulation system to avoid external disturbances that could compromise the stability of the CNTs within the bundle. The instantaneous temperature of the particles can be described using the Boltzmann theory of the mean distribution of energy [42]:

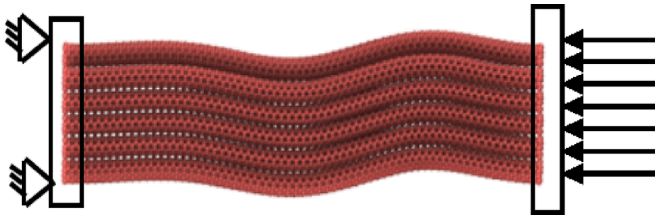

Fig. 6. Load application method on the W-VACNT bundles to simulate axial compression loading with a user-specified compression rate on top of the bundle and fixed ends at the bottom.

$$\mathbf{T}(\mathbf{t}) = \sum_{i=1}^{N} \frac{m v_{a,i}^2(t)}{(\mathrm{dim}) \bullet N \bullet K_B} \tag{6}$$

where N, m, $v_{a,i}$, dim, and K_b are the system particle number, particle mass, component velocity of *i* particle along a direction, dimensionality of the simulation (i.e., 3), and the Boltzmann constant, respectively. The W-VACNT bundle was later compressed until critical buckling was observed for a specific number of steps that were highly dependent on the bundle size and applied engineering strain rate. The complete simulation parameters are summarized in Table 2.

4. Results and discussion

4.1. Influence of waviness on the buckling behavior of W-VACNTs

The main goal of this study was to obtain insight into the buckling behavior of W-VACNT bundles relative to their size. However, the consideration of van der Waals interactions also has a strengthening effect on the load-carrying capacity of carbon nanotube bundles. Thus, the results highlight the influence of the three parameters on the buckling properties of the W-VACNT bundles, that is, waviness, bundle size, and long-range van der Waals interactions. To investigate the influence of waviness on the buckling properties of the bundles, each bundle of the samples shown in Fig. 5a was modeled at the different waviness ratios shown in Fig. 4 and listed in Table 1. Fig. 7 shows the plot of the compressive stress of a W-VACNT with 30 SWCNTs compared to each other at varying waviness ratios.

Fig. 7a presents a linear relationship between waviness and the total compressive engineering stress, which was calculated by estimating the initial cross-sectional area of the total VACNT bundle (A_0) along with the applied load (P) using the following relation.

$$\sigma_{\mathrm{comp}} = \frac{P}{A_0} \tag{7}$$

As shown in Fig. 7a, the straight bundle (w = 0.0) had the highest load-carrying capacity with a critical buckling stress σ_{comp} = 1245.2 MPa, which was slightly higher than that of the second VACNT (w = 0.06), which had a buckling stress σ_{comp} = 1048. 94 MPa. Furthermore, increasing (w) to w = 0.17 and w = 0.33 yielded critical buckling stresses of the VACNTs that significantly degraded to σ_{comp} = 1020.971 MPa and σ_{comp} = 670.732 MPa, respectively. Therefore, the critical buckling load of the bundle was estimated to decrease by 59.96% between straight (w = 0.0) and extremely wavy (w = 0.33) VACNT. As illustrated in Fig. 7b, four different regimes summarize the behavior of

Table 2
Summary of simulation parameters during relaxation and compression stage.

Relaxation Stage				
Timestep	No. of Steps	Ensemble		T_{target}
0.001 ps	20,000	NPT		300 K
Compression Stage				
Timestep	No. of Steps	Ensemble	T_{deform}	Strain rate
0.001 ps	30,000 –40000	NPT	300–1200 K	0.01/ps

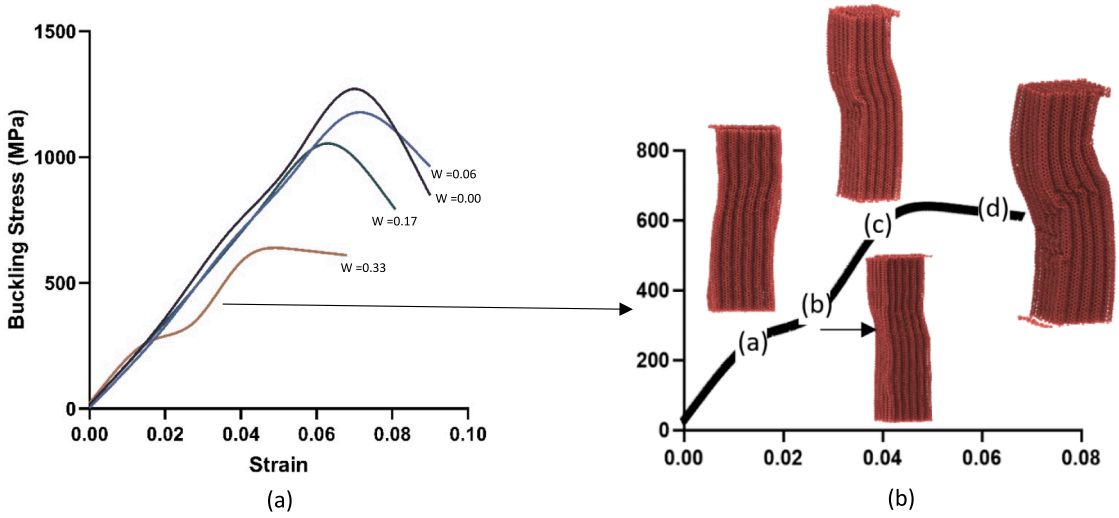

Fig. 7. A) compressive stress of w-vacnt with 30 swcnts at incremental waviness ratios along their axes, showing the influence of increasing the waviness ratio on the buckling performance of the w-vacnt bundles. b) stress–strain curve of the highest waviness vacnt (w = 0.33) highlighting the four distinct regimes of buckling behavior of the bundle.

the bundle. Region (a) highlights the linear elastic region of the bundle, and region (b) is the plateau region presented by a series of oscillatory behaviors, as indicated by [43], which might be related to the increased energy fluctuation during the loading process. Region (c) highlights the densification region, which is defined by a significant increase in buckling stress. In region (d), maximum buckling was reached by the W-VACNT bundle. To elaborate on the change in buckling behavior owing to waviness, we can visualize the buckling pattern on the four samples presented in Fig. 7. The visualization of the atomic structure is obtained using The Open Visualization Tool (OVITO) and the results are presented in Fig. 8:

It was also observed that the W-VACNT bundles exhibited progressive local buckling with incremental strain, as shown in Fig. 9.

As observed in Figs. 8 and 9, buckling begins to develop from the bottom of the W-VACNT arrays towards the top as the applied strain increases. This behavior was also reported by Li et al. [11] and Pathak et al. [43], who analyzed the local buckling behavior of VACNTs using SEM imaging. After buckling develops in the bottom region of the bundle, the buckling waves begin to progressively develop toward the top region of the VACNT array with new buckling waves propagating

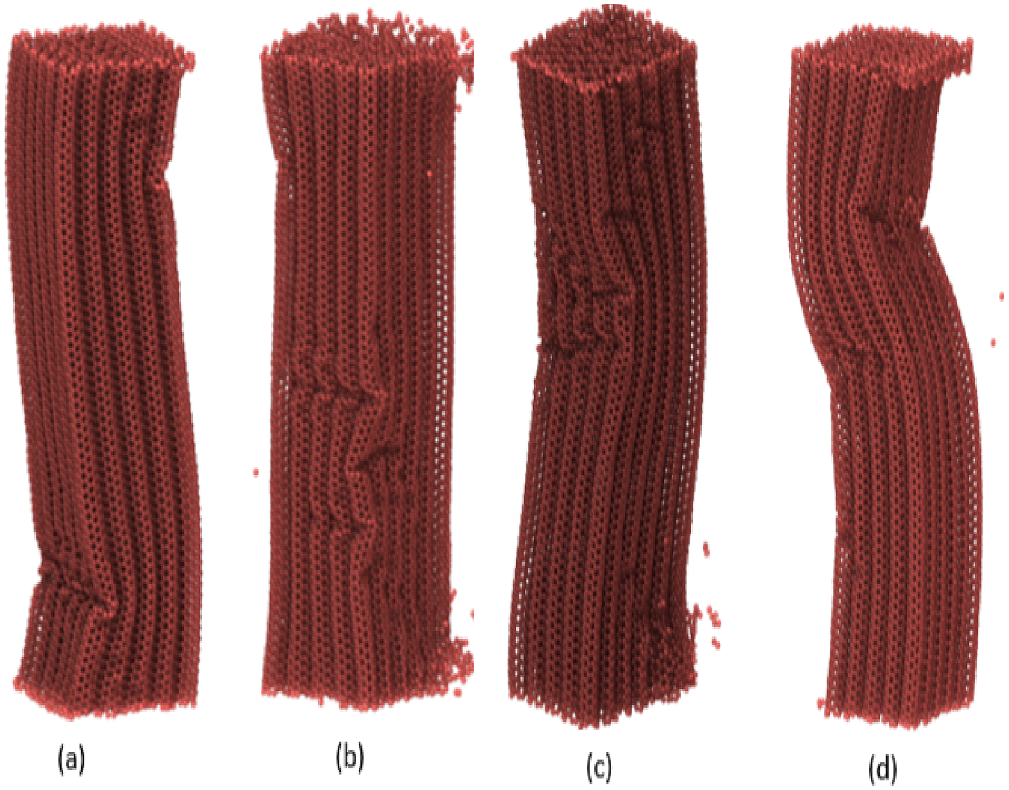

Fig. 8. Visualization of the buckling pattern of VACNTs at incremental waviness ratios where the deterioration in the structural integrity of the bundle can be visualized at increased waviness a) w = 0.00b) w = 0.06c) w = 0.17 d) w = 0.33.

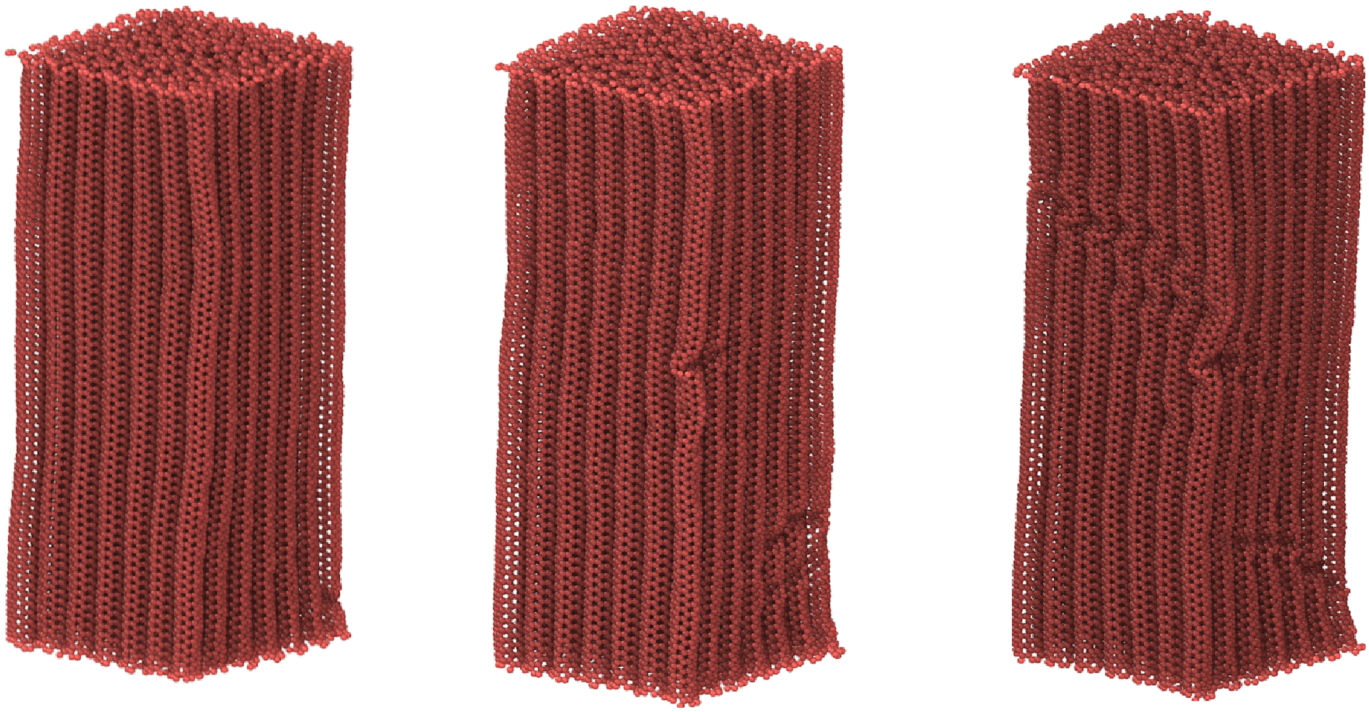

Fig. 9. Progressive buckle behavior on the W-VACNT from left to right buckling waves begin to propagate from bottom to top along the axis of the nanotubes.

upward. This buckling behavior can be attributed to several factors. However, it can be closely compared to the wave-damping effect [44]. The buckling behavior of the CNTs can be described by the symmetrical buckling of cylindrical shells under uniform axial compression. In theory, if a cylindrical shell is uniformly compressed in the axial direction several axis-symmetrical buckling waves in the longitudinal direction due to the surrounding constraining forces. Furthermore, the buckling waves decrease in amplitude as they propagate upwards until they reach zero. This is observed closely in Fig. 8b and 9, where the buckling waves propagate from the lower part of the CNT and eventually disappear upwards. Comparable to the shell buckling [45,46], the W-VACNT bundles in Fig. 8 have multiple short buckling waves that interestingly seem to have relatively constant amplitude. Moreover, the waviness highlighted in Fig. 8 suggests that the waviness present near the fixed support as highlighted in Fig. 6 does not have a considerable influence on the buckling propagation. However, the waviness along the axis in the mid-region of the bundle tends to have the greatest influence on the buckling load, as majority of the buckling waves are observed in the middle region of the W-VACNT bundle.

4.2. *Influence of van der Waals interaction on the buckling behavior of W-VACNTs*

As described in Section 3, this study also investigated the influence of VdW interactions on the buckling behavior of nanotubes. The van der Waals interaction is defined as the repulsion and dispersion forces between non-bonded atoms and molecules. Therefore, the removal of the VdW long-range interactions was isolated from the AIREBO potential by eliminating vdW interaction term from Equation 1. Fig. 10 shows the results after eliminating the vdW interaction with respect to waviness compared to the results obtained in Fig. 7 which includes the vdW interactions.

As observed in Fig. 10, it is noted that the maximum buckling stress of the bundle decreases when the van der Waals interactions are

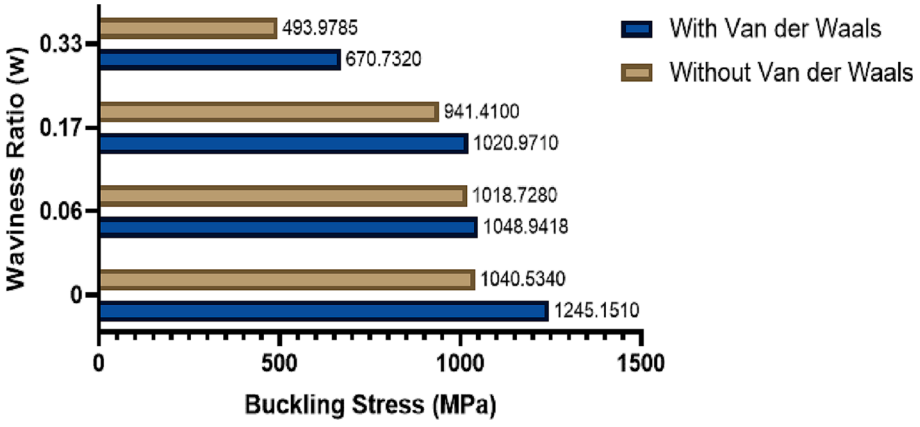

Fig. 10. The obtained critical buckling stress of the same W-VACNTs illustrated in Fig. 8 are varying waviness ratios compared to their similar counterparts without the inclusion of long-range van der Waals interaction.

eliminated, which yields the conclusion that the Van der Waals interactions play the role of strengthening the bundle. Furthermore, the presence of van der Waals interactions is highly dependent on the inter-tube spacing within the bundle; Thus, a greater inter-tube spacing requires stronger van der Waals interactions. Also, it is interesting to note that the buckling behavior of the bundle changes when the VdW interactions are eliminated. The bundle consisting of 30 VACNTs exhibited an extreme oscillatory plateau, a behavior observed by [47]. This behavior is further shown in the stress–strain curve of the bundles without VdW interactions below.

It is concluded that the implementation of van der Waals interactions between the CNTs in a bundle plays a critical role in strengthening the overall VACNT bundle rigidity, as observed by Liew et al. [48] and Gangele et al. [49]; However, The elimination of VdW interactions significantly changed the buckling pattern and behavior of the bundles. The bundles shown below buckled under the same conditions as the bundles in Fig. 8 presented along their stress–strain curve, which includes a discussion of the stress–strain curve of the sample shown in Fig. 12d that was earlier presented in Fig. 11.

From Fig. 12d, it is observed that the straight bundle with no van der Waals interactions conforms to the buckling pattern with the behavior reported by Chowdhury et al [5] which can be attributed to a Euler buckling mode. However, as the waviness increases to the maximum value, we defined it earlier in Table 1. The relatively long bundles (L = 15.9 nm) exhibit beam-like buckling, as shown in Fig. 12a, for a straight bundle. However, the increase in curvature causes the bundle in Fig. 12d to propagate zigzag buckles, which can be simply described as folded springs that regain their structure without any fracture, as opposed to the W-VACNTs in Fig. 8, which incorporated VdW interactions. This was also reported in [7]. Additionally, the presence of vdW interactions significantly influences the inter-tube spacing of the W-VACNT bundle. This is observed in Fig. 11, where the bundle without vdW interactions had larger spacing between the CNTs. Thus, the vdW interactions enhance the inter-tube interactions and eventually the overall strength of the bundle as evidenced by the decrease in buckling stress of the bundle when vdW interactions were removed.

From the stress–strain curves above, we notice a particularly important aspect that is directly proportional to the increase in waviness of the VACNTs within the bundle, which is oscillatory behavior. To elaborate, the initial stress–strain curve for the straight bundle in Fig. 13a exhibited a smooth increase in the linear elastic region of the structure; however, as we increased the waviness ratio (w) along the axis of the tubes, there was a gradual increase in the fluctuation pattern in the remaining stress–strain curves. Furthermore, the behavior observed in the curves is consistent with that reported previously [50,12]. In their studies, region (a) highlighted in Fig. 13a is the linear elastic region of the bundle with slide-buckling behavior at the peak before the post-buckling region (b). Moreover, the VACNT with w = 0.0 reported critical buckling stress of σ_{comp} = 1040.534 MPa, which is slightly lower than that of the VACNT with w = 0.0, including the VdW interactions. However, when the waviness ratio was increased to w = 0.17 and w = 0.33, the critical buckling loads of the VACNTs rapidly dropped to σ_{comp} = 941.410 MPa and σ_{comp} = 493.980 MPa, respectively. Therefore, the critical buckling load of the bundle decreased by approximately 47.52% between the straight VACNT and the extremely wavy VACNT of w = 0.0 and w = 0.33, respectively.

The change in the critical buckling stress for each of the following specimens from Figs. 5, 8, and 12 are summarized in Table 3.

Additionally, Analyzing the potential energy (PE) of the system can provide insight into the energy stored within the W-VACNT bundle. Evaluating its change against time reflects the deformation and stability of the analyzed bundle when it is subjected to compressive loading. Fig. 14 illustrates the time evolution of the potential energy of the W-VACNT bundles (samples 1–3) with vdW interactions and (samples 5–7) without vdW interactions. Furthermore, this variation of samples also gives insight into the effect of waviness on the total potential energy of the W-VACNT bundles.

Generally, the plot shows a sudden increase in PE near the buckling point of the bundle. This is because as the bundle is compressed, the interatomic distance between the CNTs is reduced; thus, increasing the PE of the system. Furthermore, at the buckling point, the compressive load-carrying capacity of the bundle reaches a maximum and buckles, which causes a sudden jump or increase in the total PE of the system. The change in PE observed in Fig. 14 gives valuable insights into the influence of the vdW long-range interactions on the stability and buckling behavior of the system. However, without the vdW interactions, the PE curve of the W-VACNT bundle under compression shows a more rapid increase in PE as the compressive strain increases. This generally indicates that the system exhibits less stability as observed in the fluctuations within the stress–strain curve of W-VACNT bundles without the vdW interaction in Fig. 13. Thus, this suggests that the presence of vdW interactions provides a stabilizing effect for the CNT configuration and eventually allowing it to resist buckling more than the bundle without vdW.

To further examine the role of vdW long-range energies in the stability and buckling behavior of the system, Fig. 15 presents the long-range energy change during compression. As observed in the plot, the long-range energy slightly increases during the compression phase, however, a sharp increase is observed as the bundle approaches the buckling region. The fact that the long-range energy is larger post-buckling compared to its value during compression might indicate permanent deformation in the W-VACNT bundle.

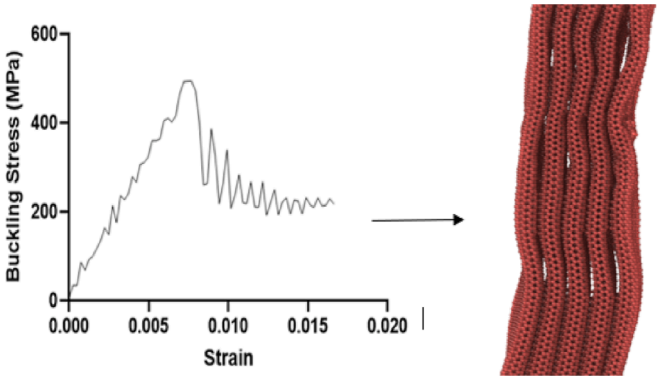

Fig. 11. Stress–strain curve of the bundle in Fig. 8c without the inclusion of VdW interactions. It is observed with high oscillatory behavior during the load application, and it is interesting to see bundles with increased gaps in between them as opposed to the same bundle with VdW interactions.

4.3. Influence of SWCNT diameter on the buckling behavior of W-VACNT

As observed in Fig. 8, the study investigated the buckling behavior of W-VACNT bundles in varying sizes, which was quantified by the number of CNTs within the bundle. However, to emphasize the structural load-carrying capacity of W-VACNT bundles, two sample bundles with larger diameters were studied under the same loading conditions. The initial diameter of the SWCNTs within each bundle presented earlier wasD_t = 6.785 Å. The samples illustrated in Fig. 16 have a diameter of D_t = 10.856 Å andD_t = 13.570 Å. Parameters such as length, chirality, and waviness ratio were kept constant.

In general, it is safe to assume that the diameter and eventually increasing surface area of the bundle have a significant impact on the overall load-carrying capacity of the CNT bundles. This can be attributed to numerous factors such as length and orientation of the SWCNTs within the bundle. Thus, the bundles illustrated in Fig. 16 were simulated under axial compressive loading using molecular dynamics simulation. Eventually, the stress–strain relation for the bundles was

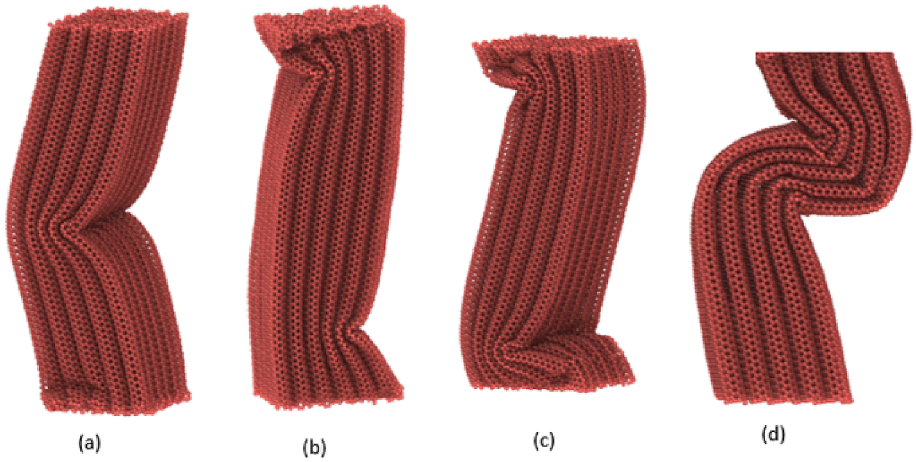

Fig. 12. Visualization of the buckling pattern of W-VACNTs at incremental waviness ratios without the inclusion of van der Waals interaction at increased waviness a) w = 0.00b) w = 0.06c) w = 0.17 d) w = 0.33.

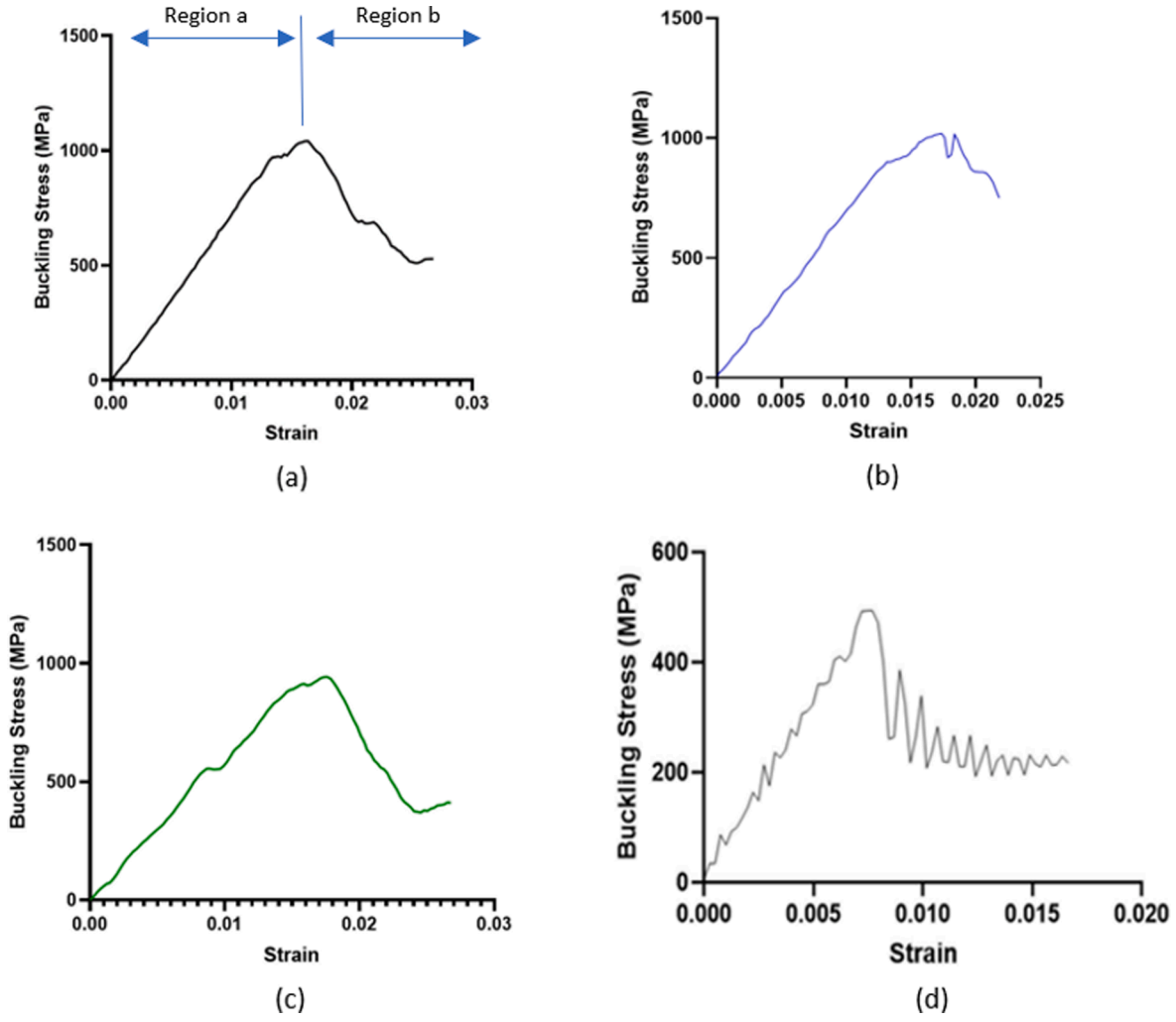

Fig. 13. Stress–strain curves of W-VACNT with 30 tubes without the inclusion of VdW interactions, at increased waviness a) w = 0.00b) w = 0.06c) w = 0.17 d) w = 0.33.

Table 3
Summary of simulation results for each W-VACNT bundle presented in the study.

Sample no.	N_{CNT}	Waviness Ratio (w)	Critical Buckling Strain (MPa)	VdW (on/off)
1	30	0.0	1245.15	on
2	30	0.060	1048.94	on
3	30	0.170	1020.97	on
4	30	0.330	670.73	on
5	30	0.0	1040.53	off
6	30	0.060	1018.73	off
7	30	0.170	941.41	off
8	30	0.330	493.98	off
9	50	0.170	1989.51	on
10	80	0.170	2461.99	on
11	50	0.170	1187.36	off
12	80	0.170	1546.93	off

obtained and compared to the bundles with smaller diameters.

Fig. 17 suggests a positive relationship between the individual SWCNT diameter within the W-VACNT bundle and the compressive load-carrying capacity of the bundle. This was consistent with the observations reported by [51,52]. The plot indicates fluctuations in the elastic region for the largest diameter bundle, which can be attributed to the vibrations induced during compression. The stress–strain curve of the larger diameter $D_t = 13.570$ shows that the bundle withstands a higher compressive load and had a critical buckling stress of $\sigma_{comp} =$ 1207.4315 MPa. The second bundle ($D_t = 10.856$ Å) yielded a critical buckling stress of $\sigma_{comp} = 1184.7017$ MPa, which is slightly lower than the previous sample which is consistent with [53]. The buckling pattern on both bundles shown in Fig. 14 is illustrated in Fig. 18:

Furthermore, this has been reported by the findings of Liew et al. [53] for the similar diameter and chirality of armchair SWCNT. In their study, the increment in diameter for armchair and zigzag SWCNT yielded an increase in the buckling load of the nanotubes. However, the tubes showed an increase in critical buckling load with diameter until an optimum diameter was reached i.e., $D_t = 11.76$ Å and $D_t = 20.36$ Å for zigzag and armchair, respectively. Since the present study investigates armchair SWCNTs, the presented samples were below the optimum range. Furthermore, it was shown by [53,54], that beyond the optimum diameter, the buckling load will decrease steadily to a steady value.

The increase in load-carrying capacity of the W-VACNT bundle with increasing diameter can be attributed to several facts such as stiffness and contact Area. Initially, an increase in the diameter of the individual SWCNTs within a bundle will cause incremental resistance to buckling under compressive loads. This is because increasing the diameter will lead to an increase in the effective bending stiffness of the overall bundle. Additionally, the increase in the diameter will result in a bigger contact area between the adjacent tubes. Thus, increasing the van der Waals interaction between them, which was shown to have a significant impact on the buckling strength of the W-VACNT bundles in Fig. 10. Observing the buckling patterns in Fig. 16 the larger diameter bundle exhibits smaller buckling waves with a large bending on the load application surface. However, the second sample $D_t = (10.856$ Å) exhibits direct buckling similar to the behavior observed in earlier samples.

5. Conclusions and future scope

In the following study, the buckling behavior of vertically aligned Carbon Nanotube (VACNTs) bundles was modeled with the normalized waviness ratio along their structure using the principle of sinusoidal waves. The bundles were generated using a MATLAB algorithm that imports straight CNTs from the VMD and generates waviness along its structure using a user-specified waviness ratio. Twelve sample VACNT models were used in the study under a constant strain of 0.01/ps uniaxial compression with three variable parameters: the waviness ratio (w), Number of VACNTs within the bundle and diameter of the CNT, and the presence of Van der Waals (VdW) interactions. The parameters significantly influenced the critical buckling stress (σ_{comp}) and buckling behavior of the bundles. Increasing the waviness resulted in a significant deterioration of the structure of the bundle with a reduction of approximately 59.96% in σ_{comp} between a bundle of w = 0.0 and a bundle with w = 0.33. Furthermore, the samples were tested while shutting off the VdW interactions to determine their influence on the buckling behavior of the VACNTs. It was concluded that the inclusion of van der Waals interactions between CNTs in a bundle plays a critical role in strengthening the overall VACNT bundle. However, eliminating the VdW interactions significantly changed the buckling pattern and behavior of the bundles from shell buckling to folded spring buckling. In addition, increasing the waviness in bundles with no VdW interactions

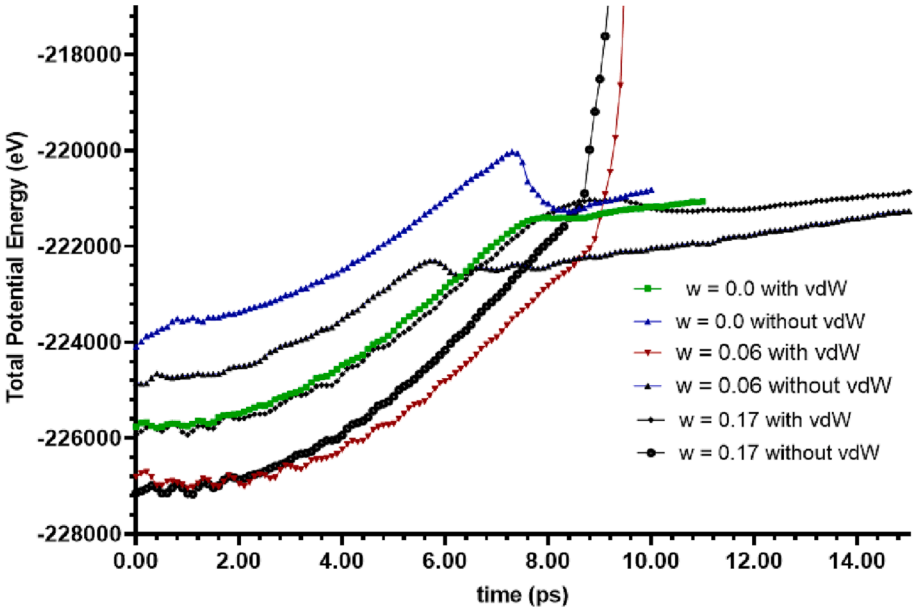

Fig. 14. Potential energy vs Time plot for W-VACNT bundles consisting of 30 SWCNTs having a constant diameter $D_t = 6.785$ Å and varying waviness ratios (W).

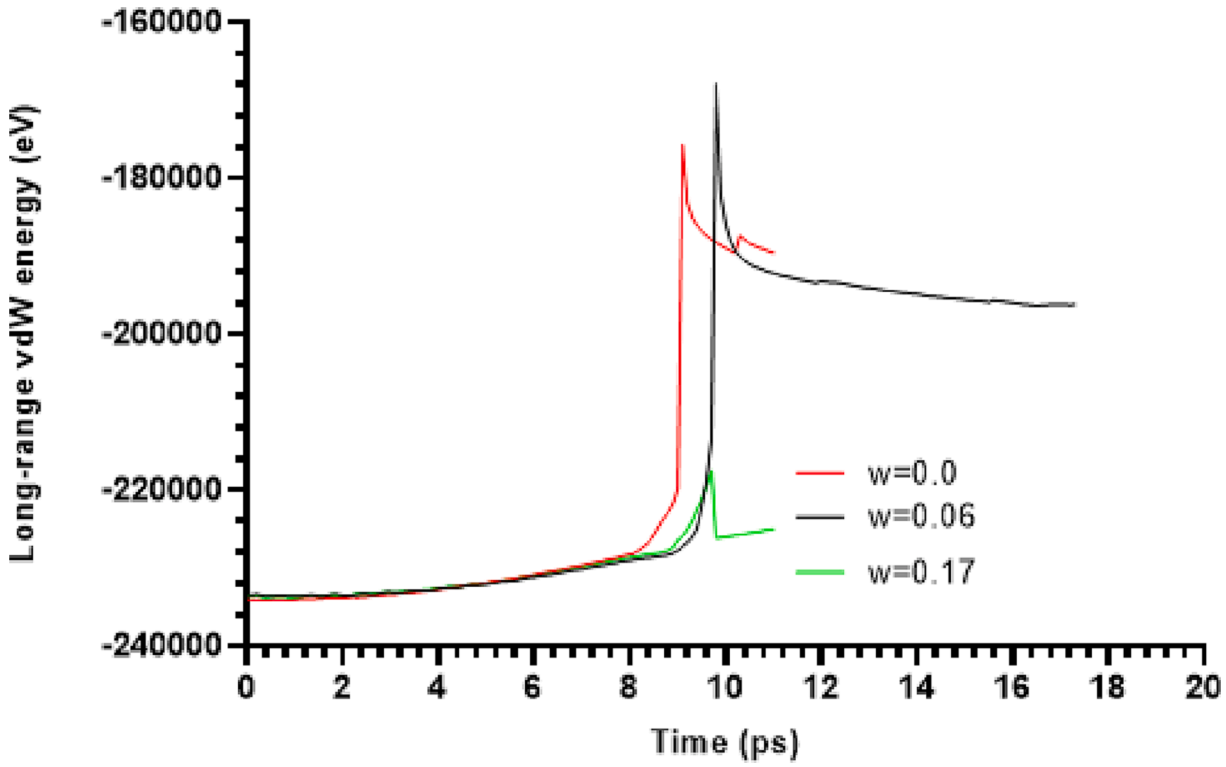

Fig. 15. Long-range energy vs Time plot for W-VACNT bundles consisting of 30 SWCNTs having a constant diameter D_t = 6.785 Å and varying waviness ratios (W) with vdW interactions activated.

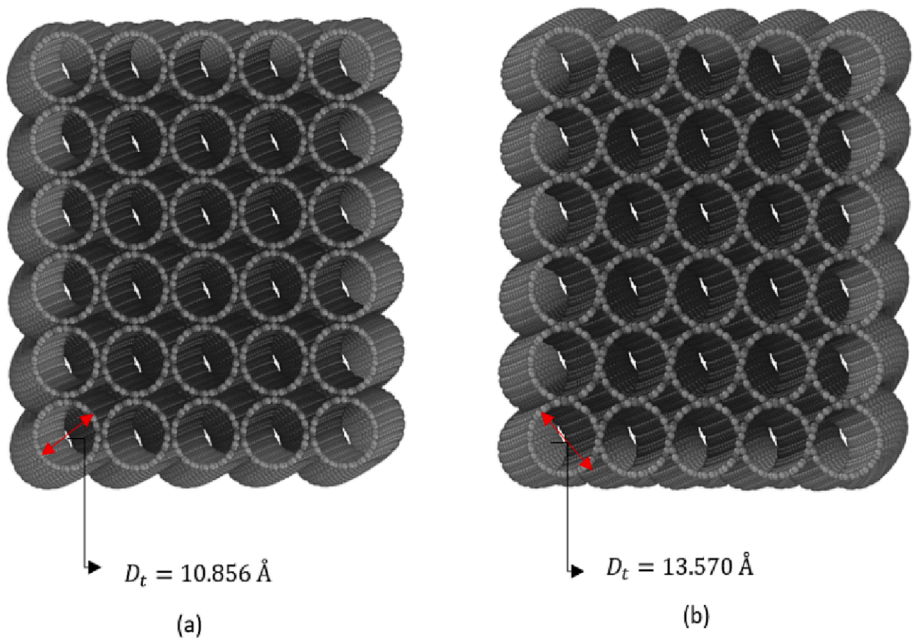

Fig. 16. W-VACNT structures with larger diameter (a) 10.856 with Chirality (8,8) Å b) 13.570 Å with Chirality (10,10) and a waviness ratio (w) = 0.170.

resulted in the propagation of an extremely oscillatory motion, as observed in the stress–strain curves in Fig. 13. Finally, we compared the buckling stress of bundles with larger surface area i.e. number of W-VACNTs, and observed a significant increase in the critical buckling stress of the overall bundle proportional to increasing the number of W-VACNTs from 30 to 50 to 80 W-VACNTs. Additionally, to emphasize the buckling behavior of W-VACNT, the study investigates the compressive load-carrying capacity of the W-VACNT bundle while varying the individual SWCNT diameter. The results suggest that the load-carrying capacity of the bundle is positively related to the individual bundle diameter, where the bundle withstands a higher compressive load.

In conclusion, the following work sets the basis for understanding the structural behavior of VACNT bundles that are expected to impact any system design in which the collective mechanical behavior of the W-VACNT bundles is critical. Furthermore, this work is expected to progress towards the implementation of composite materials within lithium-

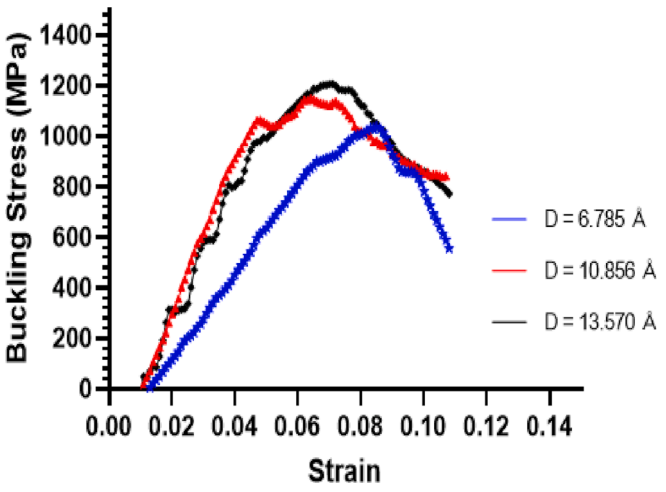

Fig. 17. Stress–strain relation for W-VACNT bundles consisting of 30 SWCNTs with Diameters $D_t = 6.785, 10.856, and 13.570$ Å.

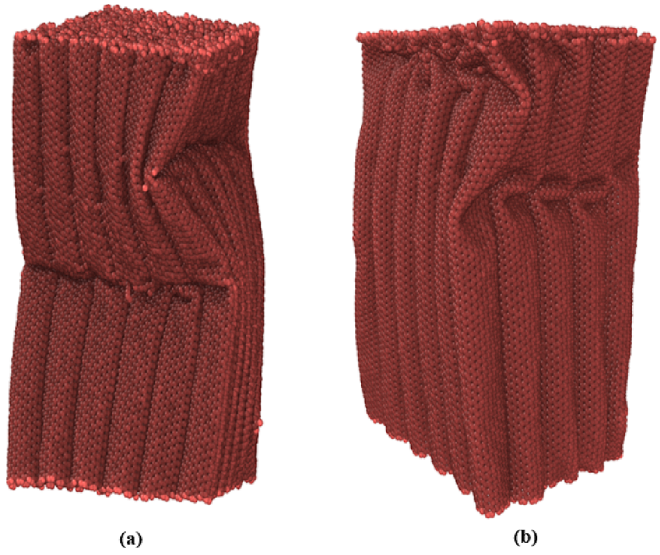

Fig. 18. Buckling pattern on W-VACNT bundles with diameter a)D_t= 10.856*b*)13.570 Å.

ion batteries for high-capacity CNT-composite anodes, which is considered a very promising application that integrates VACNT bundles into high-capacity energy storage that utilizes the remarkable thermal and electrical conductivity of the VACNTS.

CRediT authorship contribution statement

Aghyad B. Al Tahhan: Conceptualization, Methodology, Software, Writing – original draft. **Mohammad Alkhedher:** Conceptualization, Validation, Writing – review & editing, Supervision. **Abdel-Hamid I. Mourad:** Conceptualization, Validation, Writing – review & editing. **Mohamad Ramadan:** Conceptualization, Validation, Writing – review & editing, Supervision. **Mutasem A. Shehadeh:** Conceptualization, Validation, Writing – review & editing.

Declaration of Competing Interest

The authors declare that they have no known competing financial interests or personal relationships that could have appeared to influence the work reported in this paper.

Data availability

No data was used for the research described in the article.

Acknowledgements

ADU author acknowledges financial support from Abu Dhabi University's Office of Research and Sponsored Programs.

References

[1] S. Iijima, T. Ichihashi, Single-shell carbon nanotubes of 1-nm diameter, Nature 363 (1993) (1993) 603–605.
[2] N. Gupta, Carbon nanotubes: Synthesis, properties and engineering applications, Carbon Letters 29 (5) (2019) 419–447.
[3] C. Yu, L. Shi, Z. Yao, D. Li, A. Majumdar, Thermal conductance and thermopower of an individual single-wall carbon nanotube, Nano Lett. 5 (9) (2005) 1842–1946.
[4] H.J. Li, W.G. Lu, J.J. Li, X.D. Bai, C.Z. Gu, Multichannel ballistic transport in multiwall carbon nanotubes, Phys. Rev. Lett. 95 (8) (2005) 086601.
[5] S.C. Chowdhury, B. Haque, G. Swenson, J.W.G. Jr, Molecular dynamics simulations of singe-walled carbon nanotube bundle under mechanical loading, SAMPE J. 51 (3) (2015) 40–41.
[6] M. Bedewy, E.R. Meshot, A.J. Hart, Diameter-dependent kinetics of activation and deactivation in carbon nanotube population growth, Carbon 50 (14) (2012) 5106–5116.
[7] A. Cao, P.L. Dickrell, W.G. Sawyer, M.-N.-G.-N.-P. Ajayan, Super-compressible foamlike carbon nanotube films, Science 310 (5752) (2005) 1307–1310.
[8] A. Szabados, L.P. Biro, P.R. Surjan, Inter-tube interaction in carbon nanotube bundles, Phys. Rev. B 73 (19) (2006) 1–2.
[9] K.M. Liew, C.H. Wong, M.J. Tan, Tensile compressive properties of carbon nanotube bundles, Acta Mater. 54 (1) (2006) 225–231.
[10] K.M. Liew, C.H. Wong, M.J. Tan, Twisting effects of carbon nanotube bundles subjected to axial compression and tension, J. Appl. Phys. 99 (114312) (2006).
[11] Y. Li, B.W. Hyung-ick Kim, J.-B.-C. Junmo Kang, J.-D. Nam, J. Suhr, Understanding the nanoscale local buckling behavior of vertically aligned MWCNT arrays with van der Waals interactions, Nanoscale 7 (2015) 14299–14304.
[12] A. Zbib, S.D. Mesarovic, E.T. lilleodden, D. McClain, J. Jiao, D.F. Bahr, The coordinated buckling of carbon nanotube turfs under uniform compression, Nanotechnology 19 (023512) (2008).
[13] L.J.H. Shelby, B. Hutchens, J.R. Greer, In situ mechanical testing reveals periodic buckle nucleation and propagation in carbon nanotube bundles, Adv. Funct. Mater. 20 (2010) 2341–2342.
[14] M.R. Maschmann, Q. Zhang, F. Du, L. Dai, J. Baura, Length dependent foam-like mechanical response of axially indented vertically oriented carbon nanotube arrays, Carbon 49 (2) (2011) 386–397.
[15] P.A. Williams, S.J. Papadakis, A.M. Patel, M.R. Falvo, S. Washburn, R. Superfine, Fabrication of nanometer scale mechanical devices incorporating individual multi-walled carbon nanotubes as torsional springs, Appl. Phys. Lett. 82 (5) (2003) 805–807.
[16] A.M. Fennimore, T.D. Yuzvinsky, W.-Q. Han, M.S. Fuhrer, J. Cumings, A. Zettl, Rotational actuators based on carbon nanotubes, Nature 424 (6947) (2003) 408–410.
[17] S.J. Papadakis, A.R. Hall, P.A. Williams, L. Vicci, M.R. Falvo, R. Superfine, S. Washburn, Resonant oscillators with carbon nanotube torsion springs, Physics Review Letters 93 (14) (2004) 146101–146104.
[18] S.K.D. Nath, S.-G. Kim, Study of the nanomechanics of CNTs under tension by molecular dynamics simulation using different potentials, ISRN Condensed Matter Physics (2014) 1–18.
[19] M.-F. Yu, O. Lourie, M.J. Dyer, K. Moloni, T.F. Kelly, R. Ruoff, Strength and breaking mechanism of multiwall carbon nanotubes under tensile load, Science 287 (5453) (2000) 637–640.
[20] S. Iijima, C. Brabec, A. Maiti, J. Bernhol, Structural flexibility of Carbon nanotubes, J. Chem. Phys. 104 (5) (1996) 2090–2092.
[21] J.F. Waters, L. Riester, M. Jouzi, P.R. Guduru, J.M. Xu, Buckling instabilities in multiwalled carbon nanotubes under uniaxial compression, Appl. Phys. Lett. 85 (10) (2004) 1787–1789.
[22] X. Liang, J. Shin, D. Magagnosc, Y. Jiang, S.J. Park, A.J. Hart, K. Turner, D. S. Gianola, P.K. Purohit, Compression and recovery of carbon nanotube forests described as a phase transition, Int. J. Solids Struct. 122 (2017) 196–209.
[23] M. Goel, S.P. Harsha, M.P. Mishra, R.K. Mishra, Buckling failure analysis of defective carbon nanotubes using molecular dynamics simulation, J. Fail. Anal. Prev. 20 (2020) (2020) 868–881.
[24] M. Al-Khedher, C. Pezeshki, J. McHale, F. Knorr, Adaptive neuro-fuzzy modeling of mechanical behavior for vertically aligned carbon nanotube turfs, J. Mater. Sci. Technol. 27 (4) (2011) 301–308.
[25] M. Al-khedher, C. Pezeshki, J. McHale, F. Knorr, Quality classification via Raman identification and SEM analysis of carbon nanotube bundles using artificial neural networks, Nanotechnology 18 (2007).
[26] A.B. Al Tahhan, M. AlKhedher, Investigating Curvature Effect on Tensile Properties of Carbon Nanotubes, in: 2022 Advances in Science and Engineering Technology International Conferences (ASET), IEEE, 2022, pp. 1–6.

[27] C.H. Wong, V. Vijayaraghavan, Nanomechanics of imperfectly straight single walled carbon nanotubes under axial compression by using molecular dynamics simulation, Comput. Mater. Sci 53 (1) (2012) 267–273.
[28] N.J. Ginga, W. Chen, S.K. Sitaraman, Waviness reduces effective modulus of carbon nanotube forests by several orders of magnitude, Carbon 66 (2014) 57–66.
[29] B. Coto, I. Antia, M. Blanco, I. Martinez-de-Arenaza, E. Meaurio, J. Barriga, J.-R. Sarasua, Molecular dynamics study of the influence of functionalization on the elastic properties of single and multiwall carbon nanotubes, Computational Material Science 50 (12) (2011) 3417–3424.
[30] M. Al-Khedher, C. Pezeshki, J.L. McHale, F. Knorr, Empirical modeling of nanoindentation of vertically aligned carbon nanotube turfs using intelligent systems, Fullerenes, Nanotubes, Carbon Nanostruct. 20 (2012) 200–215.
[31] F.T. Fisher, R.D. Bradshaw, L.C. Brinson, Fiber waviness in nanotube-reinforced polymer composites—II: Modeling via numerical approximation of the dilute strain concentration tensor, Compos. Sci. Technol. 63 (2003) (2003) 1705–1722.
[32] X. Zeng, X. Xu, P.M. Shenai, E. Kovalev, C. Baudot, N. Mathews, Y. Zhao, Characteristics of the electrical percolation in carbon nanotubes/polymer nanocomposites, J. Phys. Chem. C 115 (44) (2011) 21685–21690.
[33] I.Y. Stien, B.L. Wardle, Influence of waviness on the elastic properties of aligned carbon nanotube polymer matrix, American Institute of Aeronautics and Astronautics (2016).
[34] K. Yazdchi, M. Salehi, The effects of CNT waviness on interfacial stress transfer characteristics of CNT/polymer composites, Compos. A Appl. Sci. Manuf. 42 (10) (2011) 1306–1309.
[35] A.R. Alian, S.A. Meguid, Molecular dynamics simulations of the effect of waviness and agglomeration of CNTs on interface strength of thermoset nanocomposites, Royal Society of Chemistry 18 (1) (2017) 1–9.
[36] T.C. O'Connor, J. Andzelm, M.O. Robbins, "AIREBO-M: A reactive model for hydrocarbons at extreme pressures,", J. Chem. Phys. 142 (2) (2015).
[37] J.E. Lennard-Jones, On the determination of molecular fields.—I. From the variation of the viscosity of a gas with temperature, Proc. R. Soc. Lond. Ser. A 106 (738) (1924) 441–462.
[38] J.E. Lennard-Jones, On the determination of molecular fields.—II. From the equation of state of a gas, Proc. R. Soc. Lond. Ser. A 106 (738) (1924) 463–477.
[39] S. Corporation, "pair_style airebo command¶," 2022. [Online]. Available: https://docs.lammps.org/pair_airebo.html#oconnor.
[40] S. Plimpton, A. Thompson, S. Moore, A. Kohlmeyer and R. Berger, "Minimize Command," Sandia National Labs, 2022. [Online]. Available: https://docs.lammps.org/minimize.html.
[41] S. Plimpton, A. Thompson, S. Moore, A. Kohlmeyer and R. Berger, "fix deform command," Sandia National Labs , 2022. [Online]. Available: https://docs.lammps.org/fix_deform.html. [Accessed July 2022].
[42] F. Chenxin, C. Yunfei, J. Jiwei, Molecular dynamics simulation of the test of single-walled carbon nanotubes under tensile loading, Science in China Series E: Technological Sciences 50 (2007) 7–17.
[43] S. Pathak, N. Mohan, E. Decolvenaere, A. Needleman, M. Bedewy, A.J. Hart, J. R. Greer, Local relative density modulates failure and strength in vertically aligned carbon nanotubes, ACS Nano 7 (10) (2013) 8593–8604.
[44] S.P. Timoshenko, J.M. Gere, Theory of elastic stability, Courier Dover Publications (2009).
[45] N. Jaunky, N.F.K. Jr, An assessment of shell theories for buckling of circular cylindrical laminated composite panels loaded in axial compression, Int. J. Solids Struct. 36 (25) (1999) 3799–3820.
[46] D. Karagiozova, M. Alves, N. Jones, Inertia effects in axisymmetrically deformed cylindrical shells under axial impact, Int. J. Impact Eng 24 (10) (2000) 1083–1115.
[47] Y. Li, H.-I. Kim, B. Wei, J. Kang, J.-B. Choi, J.-D. Nam, J. Suhr, Understanding the nanoscale local buckling behavior of vertically aligned MWCNT arrays with van der Waals interactions, Nanoscale 7 (34) (2015) 14299–14305.
[48] K.M. Liew, C.H. Wong, M.J. Tan, Buckling properties of carbon nanotube bundles, Appl. Phys. Lett. 87 (2005) 041901–041903.
[49] A. Gangele, S.K. Garala, A.K. Pandey, Influence of van der Waals forces on elastic and buckling characteristics of vertically aligned carbon nanotubes, Int. J. Mech. Sci. 146 (2018) 191–199.
[50] L. Liu, G. Cao, X. Chen, Mechanisms of nanoindentation on multiwalled carbon nanotube and nanotube cluster, J. Nanomater. 2008 (2008) 271763.
[51] C. Li, T.-W. Chou, Modeling of elastic buckling of carbon nanotubes by molecular structural mechanics approach, Mech. Mater. 36 (11) (2004) 1044–1055.
[52] F. Mehralian, Y.T. Beni, Y. Kiani, Molecular dynamics study on the thermal buckling of carbon nanotubes in the presence of pre-load, Mater. Res. Express 4 (1) (2017) 015011.
[53] K.M. Liew, C.H. Wong, X.Q. He, M.J. Tan, S.A. Meguid, Nanomechanics of single and multiwalled carbon nanotubes, Phys. Rev. B 69 (11) (2004) 115429–115437.
[54] L. Chen, Q. Zhao, H. Zhang, Axial buckling behavior of single-walled carbon nanotubes with finite element modeling, in: 2010 IEEE 5th International Conference on Nano/Micro Engineered and Molecular Systems, IEEE, 2010, pp. 276–279.